Advances in Aerodynamics

RESEARCH

Open Access

Numerical study on the combustion process in a gas turbine combustor with different reference velocities

Cheng Gong[1], Shufan Zhao[1], Weiqiang Chen[1*], Wenyu Li[1], Yu Zhou[1] and Ming Qiu[1]

*Correspondence:
chenweiqiang@cardc.cn

[1] Aerospace Technology Institute, China Aerodynamics Research and Development Center, Mianyang 621000, China

Abstract

The mixing and combustion processes under different reference velocities in a gas turbine combustor were numerically investigated using the Flamelet Generated Manifold (FGM) model based on the Reynolds Averaged Navier–Stokes (RANS) method. The flow and combustion fields show strong self-similarity except on the slow auto-ignition in the mixing layer between fuel-rich product and fresh air upstream of the flame stabilization position. The time-scale analysis was carried out to understand the combustion modes inside the combustor. In general, the residence time of the fuel-mixture is much longer than both the chemical time scale and the mixing time scale. Thus, the combustion properties in each sub-zone were dominated by the mean flow structures. Furthermore, the combustion process exhibits a mixing-controlled feature in total. However, partially premixed combustion still appears on the flame base. Most of the fuel was found to be oxidized in the primary zone and the intermediate zone; however, the slow oxidization reactions also play a non-negligible role on the whole combustion process. Finally, a sketch map on the space of mixture fraction and combustion efficiency was proposed to understand the mixing and oxidization experiences of the fuel mixture.

Keywords: Gas turbine combustor, Swirling flame, FGM, Combustion mode, Time-scale analysis

1 Introduction

One of the most important parts of an aircraft gas turbine is the combustor, which increases the thermal energy of a stream of moving air through combustion. Due to their excellent performance in terms of ignition and flame stabilization, swirling flames are widely used in modern gas turbine combustors. In a swirling combustor, the flame is anchored by imparting an azimuthal component to the flow (usually by passing the airstream through a swirler). The rotation induced by these devices generates a central recirculation zone (CRZ) and, in many cases, an outer recirculation zone filled with hot combustion products, which serves as a continuous ignition source to stabilize the flame [1]. The flow and combustion behaviors of confined swirling flames with liquid fuels are of technical and fundamental interest. Numbers of experimental

rigs have been designed, and optical diagnostics have been carried out to investigate the swirling flame under aero-engine relevant conditions [2–6]. Numbers of numerical works (e.g., Refs. [7–9]) targeted to these laboratory combustors have also been carried out to improve the understanding on the combustion process in aero-engines.

To extend the operating range, lateral air jets are implemented as well as the swirling airflow in the real aero-engine combustors [10]. As a result, the region inside the combustor is further divided into several sub-zones by the lateral air jets. These are the primary zone, the intermediate zone, and the dilution zone [11]. The laboratory combustors were usually simplified for optical diagnostics. Among the above research, the flow and flame structures downstream of the swirler, which corresponds to the primary zone, have been investigated. Due to the complexity of geometry, most of the research works on real combustors (e.g., Refs. [12–14]) focused on the global performances, including the combustion efficiency, lean blow-out limit, total pressure recovery, and temperature pattern at the outlet. However, little attention was focused on the combustion characteristics in the intermediate zone and the dilution zone, which could also have effects on the combustion efficiency.

Among the flow parameters in the combustor design, the reference velocity [11], which is defined as the mean velocity across the plane of the maximum cross-sectional area of the casing in the absence of liner, is important to determine the radial scale of the combustor. The radial scale of the combustor directly affects the specific windward area thrust of the engine, which is crucial to the flight speed of the aircraft. On the other hand, incrementing the reference velocity may increase the challenges of combustion stabilization and efficiency.

Computational fluid dynamics (CFD) is a powerful tool in the research of the aero-engine combustor. However, the Direct Numerical Simulation (DNS) and Large-Eddy Simulation (LES) are still too expensive on the CPU hour cost and computational period for the engineering design. On the other side, Reynolds-averaged Navier–Stokes (RANS) simulation is computationally efficient and is widely employed in the design. Models on the interaction of combustion and turbulence (the so-called "turbulent combustion model") are the most important model on the accuracy of the modeling. The Flamelet Generated Manifold (FGM) model developed by Van Oijen and De Goey [15] has emerged as an attractive approach for simulating combustion in gas turbine combustors, contributing to its less computational resource requirements. It has been well-validated for the confined swirling spray flame in gas turbine combustors [14, 16, 17]. Since the thermal properties (including the compositions and temperature) of the flame are tabulated based on the mixture fraction and reaction progress, the computational cost is free on the chemical kinetics, which makes it possible to involve detailed chemical kinetics in the modeling of the real combustor.

Motioned by the above discussions, the FGM model coupled with the RANS method is used to investigate the combustion process in a small-scale combustor with a high reference velocity. The objectives of this study are to delineate the effect of the reference velocity on the combustion process and to improve understanding of the combustion modes inside the combustor, which aim to provide technical guidance for further optimization of the combustor.

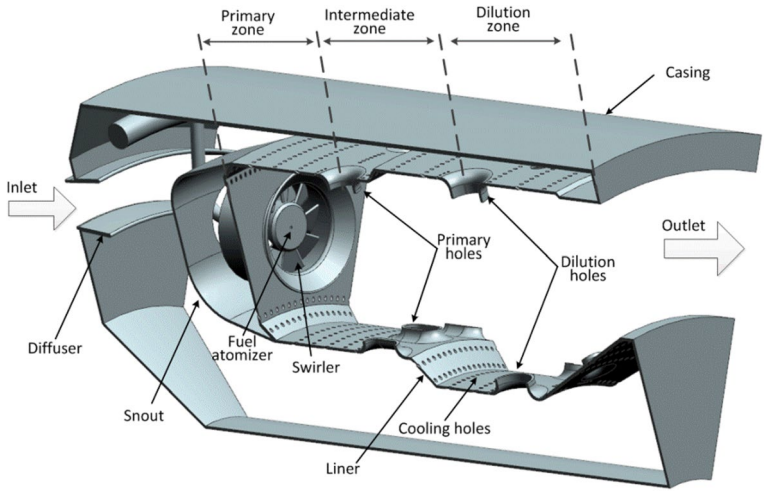

Fig. 1 Single sector geometry of the studied combustor

Table 1 Operation conditions for the simulations

	U_{ref} [m/s]	P [atm]	T_{inlet} [K]	FAR [-]
Case 1	25	6.5	540	0.018
Case 2	8	6.5	540	0.018

2 Combustor geometry and numerical setup

The study object in the present work is an annular swirling combustor designed for a small-scale turbojet engine with high specific area thrust. To improve the specific area thrust of the engine, the reference velocity of the combustor at the designed point is around 25 m/s, which is much higher than the combustor for a similar-scale engine. The combustor contains 12 same sectors. As shown in Fig. 1, the combustor is characterized by an inlet diffuser, snout, liner, swirler, fuel injector, and casing. A single-stage swirler with an installing angle of 60° is used for flame stabilization. The liquid kerosene is used as the fuel. A hollow-cone atomizer with an 80° spray angle is used for fuel injecting. The thickness of the liner is 1 mm. The discrete-hole film with a diameter of 1 mm is used to cool the liner. The primary air holes and the dilution holes divide the inside region of the liner into three sub-zones: primary zone, intermediate zone, and dilution zone. The operation conditions for the present study are listed in Table 1. Two cases with only a difference in the reference velocity are considered, in which the case with a high reference velocity corresponds to the designed point of the combustor.

The flow and combustion processes are modeled using the commercial CFD software ANSYS Fluent [18]. The coupled Eulerian-Lagrangian approach is used to model the double-phase flow process, in which the flow and combustion in the gas phase are solved in the Eulerian frame; the atomization and evaporation processes of the liquid fuel are modeled in the Lagrangian frame. The flow and spatial transport of the gas phase are solved on the steady RANS frame with the realizable k-epsilon model. The FGM model is employed for the interaction of turbulence and combustion, in which the flame structure is described using the mixing fraction (z) and the reaction progress variable

(c) based on the flamelet assumptions [19]. The flame tabulation for the FGM model is generated based on the diffusion flamelet equations [19]. Beta-shape probability density function (PDF) is assumed for the fluctuations of both the mixture fraction and the progress variable. Following the sensitivity studies carried out by Ihme et al. [20] and Yadav & Nakod [21], the reaction progress variable is defined based on CO_2 and CO mass fractions. The reaction progress variable and the normalized reaction progress are defined as

$$\begin{aligned} Y_c &= Y_{CO_2} + Y_{CO}, \\ c &= \frac{Y_c}{Y_c^{eq}(z)}, \end{aligned} \tag{1}$$

where Y_c^{eq} is the reaction progress variable under the chemical equilibrium state, and is a function of mixture fraction (z). In the RANS simulation, the turbulent flame structures are modeled by transporting the mixture fraction, the unnormalized reaction progress variable, and their variances, expressed as

$$\begin{aligned} \frac{\partial \overline{\rho}\tilde{z}}{\partial t} + \frac{\partial}{\partial x_i}\left(\overline{\rho}\tilde{u}_i\tilde{z}\right) &= \frac{\partial}{\partial x_i}\left(\overline{\rho}(\tilde{D}+D_t)\frac{\partial \tilde{z}}{\partial x_i}\right) + \overline{S}_{z,evp}, \\ \frac{\partial \overline{\rho}\tilde{Y}_c}{\partial t} + \frac{\partial}{\partial x_i}\left(\overline{\rho}\tilde{u}_i\tilde{Y}_c\right) &= \frac{\partial}{\partial x_i}\left(\overline{\rho}(\tilde{D}+D_t)\frac{\partial \tilde{Y}_c}{\partial x_i}\right) + \overline{\rho}\widetilde{\dot{\omega}_{Y_c}}, \\ \frac{\partial \overline{\rho}\widetilde{z''^2}}{\partial t} + \frac{\partial}{\partial x_i}\left(\overline{\rho}\tilde{u}_i\widetilde{z''^2}\right) &= \frac{\partial}{\partial x_i}\left(\overline{\rho}(\tilde{D}+D_t)\frac{\partial \widetilde{z''^2}}{\partial x_i}\right) + c_1\mu_t\left|\nabla\widetilde{z''^2}\right| - c_2\overline{\rho}\tilde{\chi}_z, \\ \frac{\partial \overline{\rho}\widetilde{Y_c''^2}}{\partial t} + \frac{\partial}{\partial x_i}\left(\overline{\rho}\tilde{u}_i\widetilde{Y_c''^2}\right) &= \frac{\partial}{\partial x_i}\left(\overline{\rho}(\tilde{D}+D_t)\frac{\partial \widetilde{Y_c''^2}}{\partial x_i}\right) + c_1\mu_t\left|\nabla\widetilde{Y_c''^2}\right| - c_2\overline{\rho}\tilde{\chi}_{Y_c} + \widetilde{Y_c''\dot{\omega}_{Y_c}''}. \end{aligned} \tag{2}$$

The mean normalized reaction progress variable is calculated as

$$\tilde{c} = \frac{\tilde{Y}_c}{\tilde{Y}_c^{eq}\left(\tilde{z}, \widetilde{z''^2}\right)}, \tag{3}$$

where $\tilde{Y}_c^{eq}$ is the function of the local mean mixture fraction and its variance, and is pre-tabulated in the FGM model. All the thermodynamic properties (e.g., the mass fraction, temperature, density, et al.) are pre-tabulated as a function of the mean mixture fraction, the mean reaction progress variable, and their variance. Take the species mass fraction as an example:

$$\tilde{Y}_i = \tilde{Y}_i\left(\tilde{z}, \widetilde{z''^2}, \tilde{c}, \widetilde{c''^2}\right). \tag{4}$$

The discrete phase model in the steady formula is implemented to model the motions of the liquid fuel, in which the atomization of the liquid fuel is ignored, and a constant diameter is assumed for the liquid particles during their lifetime in the combustor. The details on numerical methods can be found in Ref. [22]. A detailed chemical mechanism with 203 species and 1592 element reactions [23] was employed to generate the FGM table.

The simulations consider one of the annual sectors with periodic boundary conditions. The meshing package, named "Fluent Meshing", in the ANSYS Fluent [18] is employed

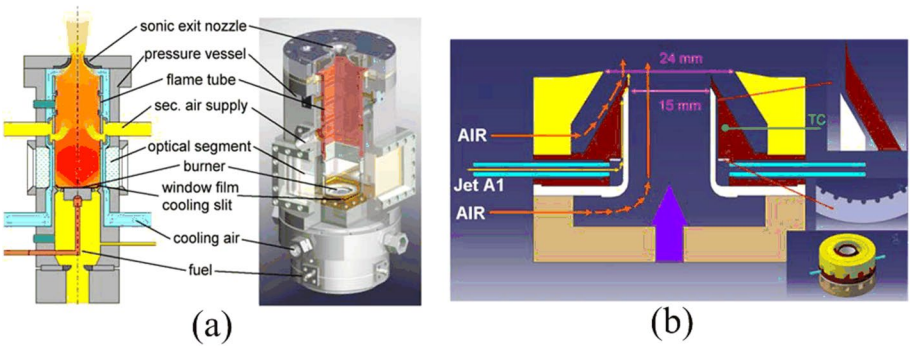

Fig. 2 Schematics of the DLR Generic Single Sector Combustor. **a** Geometry of the experimental rig. **b** Geometry of the burner

Table 2 Operation conditions on the DLR combustor

Case	Air pressure [MPa]	Air Temperature [K]	Burner air flow [g/s]	Cooling air flow [g/s]	Fuel flow [g/s]
Isothermal	0.4	295	82	0	0
Reactive	1.0	650	140	39	6.8

to generate the mesh for CFD simulations, in which the computational domain is discretized using tetrahedral cells. The mesh is locally refined around and inside the combustor liner. The minimal grid size is 0.25 mm; the grid size inside the combustor liner is limited in 2 mm. Around 9.2 million cells in total are used for the mesh. The mass flow rate and temperature are fixed at the inlet; the pressure boundary is set up for the outlet; the adiabatic wall boundary is set up for the diffuser, casing, swirler, and liner. The computations were carried out on the high-performance computers in the National Supercomputer Center in Guangzhou with 32 CPUs. Around 1000 CPU hours were consumed for each case.

3 Model validation

3.1 Evaluation on the DLR model combustor

The numerical methodology is first evaluated on the DLR Generic Single Sector Combustor (GENRIG). The details on the model combustor can be found in Refs. [6, 24]. As shown in Fig. 2a, the model combustor features a square cross section of 102×102 mm^2 and a length of 264 mm. Electrically preheated compressed primary air (marked as yellow color in Fig. 2a) was supplied to the plenum upstream from the combustor chamber. Additional preheated air was diverted from the primary air and guided to the windows for cooling. The secondary air supply shown in the figure was not used in the present conditions. As shown in Fig. 2b, the burner contains a co-rotating double stage air swirler coupled with a pre-filming fuel injector. The liquid kerosene is used as the fuel in the experiment. The isothermal and reactive cases are modeled in the present evaluation. The operation conditions are listed in Table 2. Following the work of Jones et al. [7], the cooling air is omitted in the present simulation since the cooling holes are located downstream to the interested region. The same method as used in the partial combustor

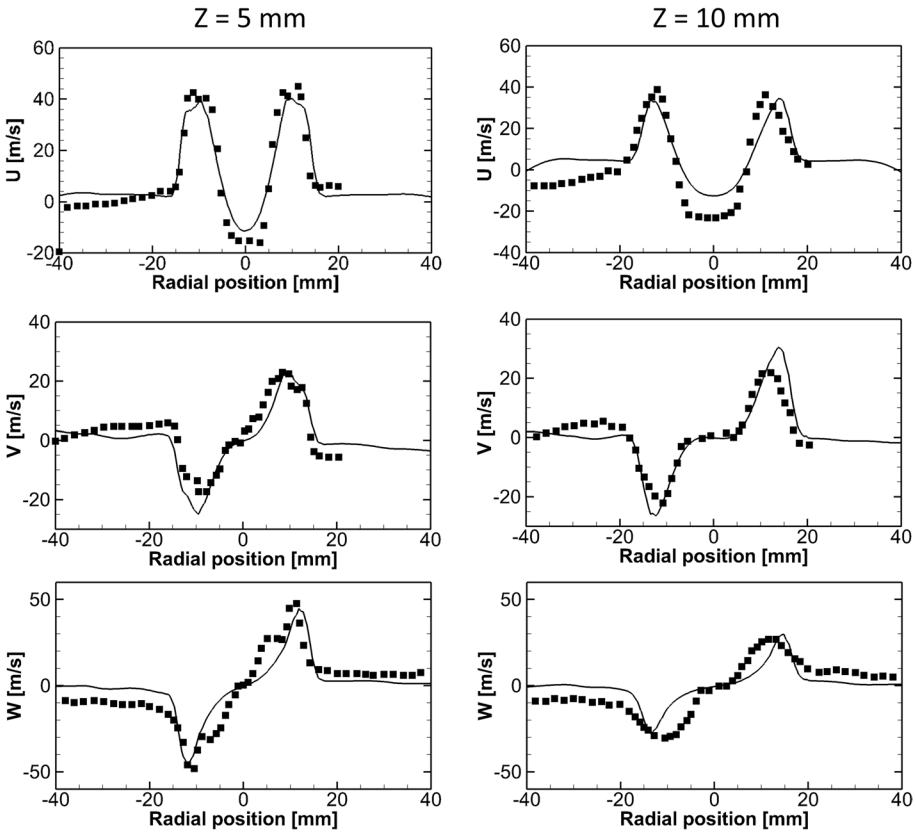

Fig. 3 Radial profiles of the axial, radial and tangential mean velocities from the isothermal case. Squares represent the experimental results from Refs. [6, 24]

is used to discretize the present simulated domain, which results in an instructed mesh with around 5.2 million cells.

Figure 3 shows the comparison of the measured [6, 24] and simulated profiles of the axial, radial, and tangential velocities at planes normal to the combustor axis at two locations ($z=5$ mm and 10 mm) for the isothermal case. It is shown that the predicted profiles of the three velocity components agree well with the measured data. Both the size of the recirculation zone and the magnitude of the velocity components are accurately reproduced. Figure 4 compares the simulated result with the experimental measurements [6] for the reactive case. The temperature in the experiment was measured by a two-line Planar Laser-induced Fluorescence (PLIF) [25]. The present method can capture the combustion feature reasonably under the present conditions, e.g., the "V-shape" of flame structure, the magnitude of temperature at the reaction region, and the lift-off at the flame base. Overall, the present numerical methods can reasonably predict the combustion process for the confined swirling spray flames.

3.2 Sensitivity study on the θ-parameter

To further evaluate the numerical methods, the sensitivity of combustion efficiency to the burner load is studied. The burner load is described by the well-known "θ-parameter" [11], which is defined as

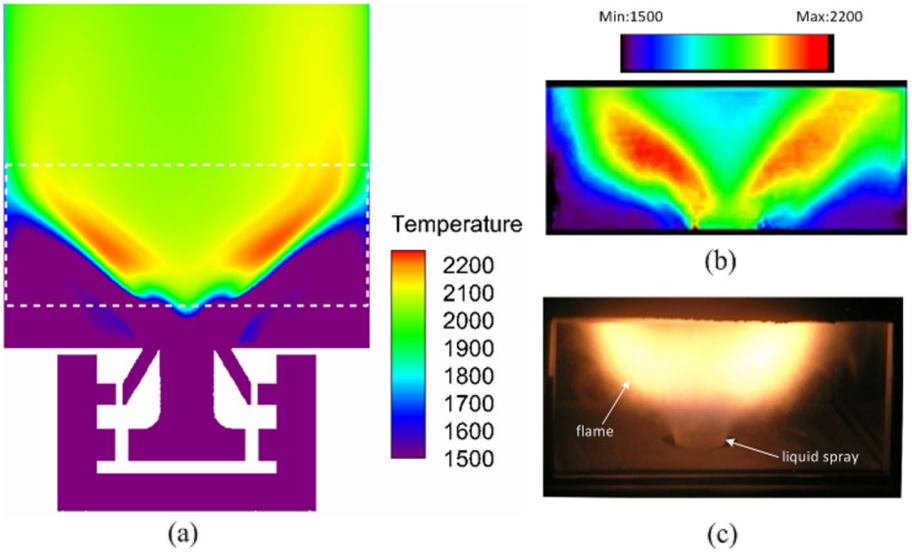

Fig. 4 Comparison of the numerical result with the experimental measurement for the reactive case: **a** temperature distribution from simulation; **b** temperature distribution based on the OH_PLIF measurement; **c** photographs of flame. The experimental result from Ref. [6]. The white box dash corresponds to the measuring window in the experiment

Table 3 Operation conditions for the θ-parameter sensitivity study

No	P [atm]	T_{inlet} [K]	U_{ref} [m/s]	θ-parameter
1	0.5	300	25	6.65×10^6
2	0.5	300	18	9.23×10^6
3	1	300	25	1.12×10^7
4	0.5	400	25	1.24×10^7
5	1	300	18	1.55×10^7
6	1	400	25	2.08×10^7
7	0.5	538	25	2.63×10^7
8	1	538	25	4.43×10^7
9	0.5	538	10	6.59×10^7
10	6.5	400	25	8.47×10^7

$$\theta = \frac{p^{1.75} A_{ref} D_{ref}^{0.75} \exp(T_{in}/300K)}{\dot{m}_{air}}. \tag{5}$$

All the parameters in the equation are in the SI units. As listed in Table 3, the θ-parameter varies between 6.65×10^6 and 8.47×10^7 by varying inlet pressure, temperature, and reference velocity, and the fuel-to-air ratio (FAR) is kept at a constant of 0.018 in the present sensitivity study. The combustion efficiency of the fuel is integrated at the combustor outlet. The combustion efficiency is defined based on the "C" atom, which is expressed as

$$\eta_c = \frac{\dot{m}_{CO_2}/M_{CO_2} + 0.531\dot{m}_{CO}/M_{CO}}{\dot{m}_z/M_{fuel} \cdot N_{C,fuel}}, \tag{6}$$

where $\dot{m}_i$ is the mass flow rate of the "i" specie on the slice; M_i is the molecular weight of the "i" specie. $N_{C,fuel}$ is the "C" atom number in the fuel molecule. The coefficient of 0.531 is referred to Ref. [26, 27], which assumes that 53.1% of the thermal power is released when the carbon atom is oxidized from kerosene to carbon monoxide (CO).

Figure 5 shows the combustion efficiency with different values of the θ-parameter. The shadow regions in the figure indicate the empirical trend summarized based on a large number of experiments with varying combustion chambers [11]. The combustion efficiency predicted based on the present method shows a similar trend to the empirical trend. There is a critical value on the θ-parameter for combustion efficiency. When the θ-parameter is below the critical value, the combustion efficiency decreases quickly with the decreasing of the θ-parameter; the combustion efficiency shows independence on the θ-parameter when it is above the critical value, and the combustion efficiency is close to 100%. The critical value for the present combustor predicted by the present model is around 2×10^7, which is close to the empirical value. The predicted combustion efficiency is slightly higher than the empirical value. A possible reason for this difference may be the ignorance of the fuel atomization effect under different aerodynamic conditions in the present numerical method. However, the values of the θ-parameter for the studied cases listed in Table 1 are much higher than the critical value (1.80×10^8 and 5.64×10^8), which indicates that the present numerical method is reliable for the studied cases in the present work.

4 Results and discussion

4.1 Results on the combustion and flow fields

Air flow distributions of the combustor liner under different conditions are listed in Table 4. The air distributions with different reference velocities are almost the same. Only slight differences in the air flow portion exist for the swirling air and the cooling air. The relative difference of the air flow is limited to 1.2%, which reveals the self-similarity

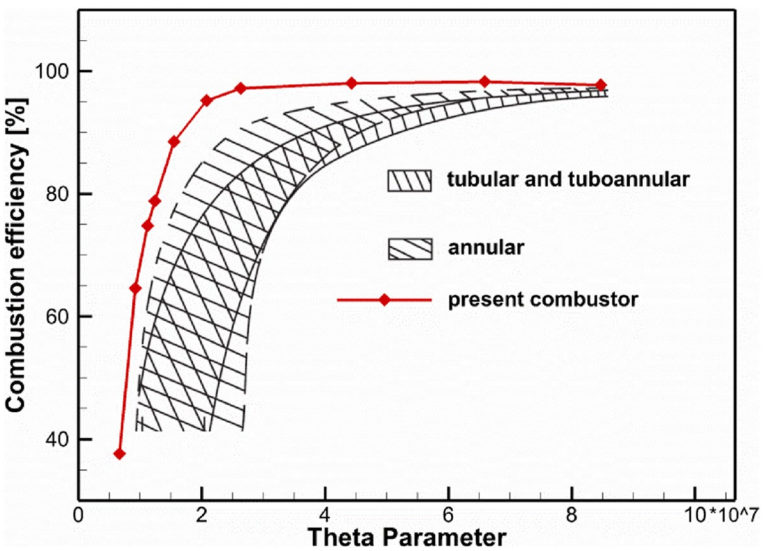

Fig. 5 Combustion efficiency versus the θ-parameter. The shadow regions in the figure indicate empirical distributions summarized in Ref. [11]

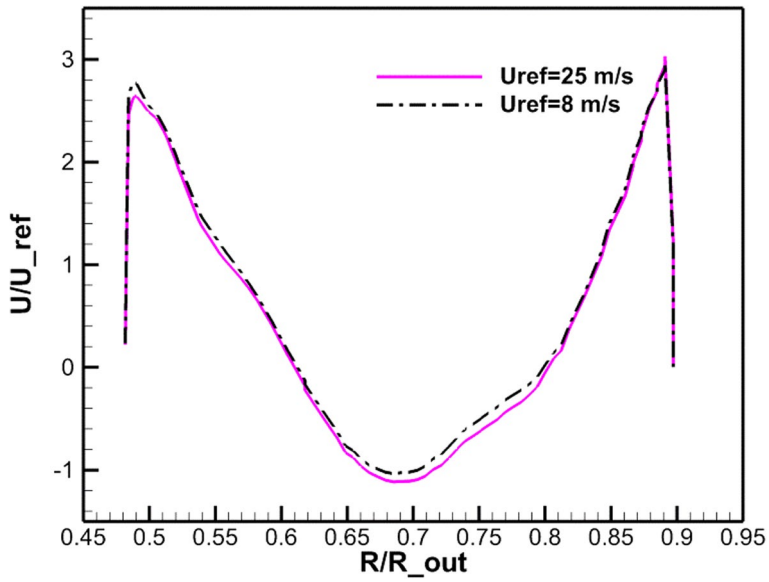

Fig. 6 The axial velocity profile at $x = 30$ mm ($x = 0$ at the outlet of the swirler)

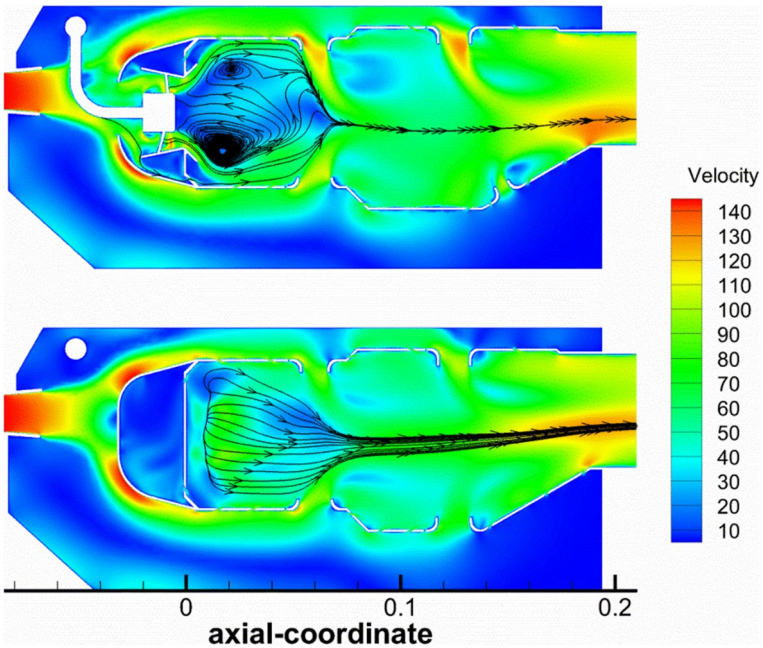

Fig. 7 The velocity distribution with $U_{ref} = 25$ m/s

of the flow field under the present conditions. The profiles of the normalized axial velocity shown in Fig. 6 further prove this conjecture. Figure 7 shows the velocity field on the middle and side planes. The velocity distributions are similar to each other for case 1 and case 2. For brevity, only the velocity distribution in case 1 is shown in Fig. 2. The streamlines in the figure show that a large-scale recirculation zone with a dual-vortex structure is generated in the primary zone on the middle plane. Since the air flow in the

Table 4 Air flow distributions under different conditions

	Swirling air	Primary air	Dilution air	Cooling air
Case 1	17.1%	24.2%	30.9%	27.8%
Case 2	17.3%	24.2%	30.9%	27.6%

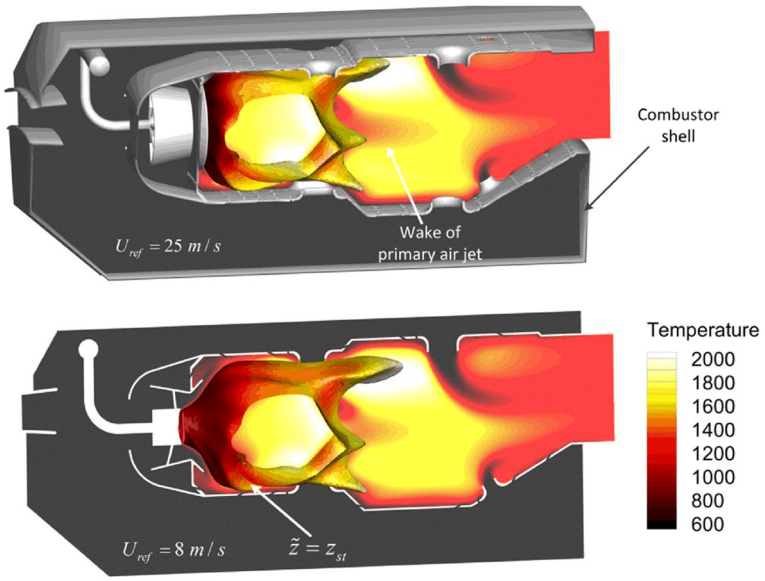

Fig. 8 The temperature distribution on the mid plane and the iso-surface of $\tilde{z} = z_{st}$

primary zone is mainly from the swirler passage, the streamlines on the side plane show a "point source" on the side plane. The recirculation zone is key to flame stabilization in the swirling combustor [11]. The flow jets from the primary holes penetrate the center of the combustor. The primary air jets can generate low-speed regions in the intermediate zone, which can improve the combustion in the intermediate zone.

Figure 8 shows the temperature distributions on the middle plane and the iso-surface of $\tilde{z} = z_{st}$. The high-temperature mixture is distributed in the primary and intermediate zones, which agrees well with the design concept of the swirling combustor. The geometry of the iso-surface in the figure shows that the fuel-rich mixture based on the mean mixture mainly exits in the primary zone. The temperature distributions are also similar to each other for the cases with different reference velocities. However, some slight differences can also be identified from the figure. For example, the wake of the primary jets is longer for the case with a high reference velocity. The angular averaged temperature and normalized axial velocity shown in Fig. 9 further validate the sef-similarity of the combustion field under the present conditions.

The combustion efficiency integrated at different axial positions is plotted in Fig. 10. Overall, the combustion reaction mainly occurs in the primary and intermediate zones. In detail, only about 65% of the injected fuel is combusted inside the primary zone; about 30% of the fuel is combusted in the intermediate zone; the slight net fuel is consumed in the dilution zone. Based on the curve in Fig. 10, the main effect of the reference velocity

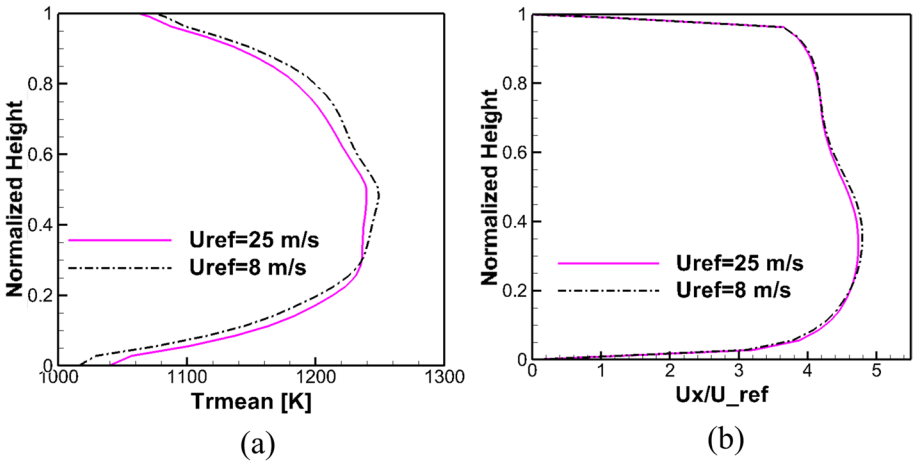

Fig. 9 Profiles of angular averaged temperature and velocity at the outlet

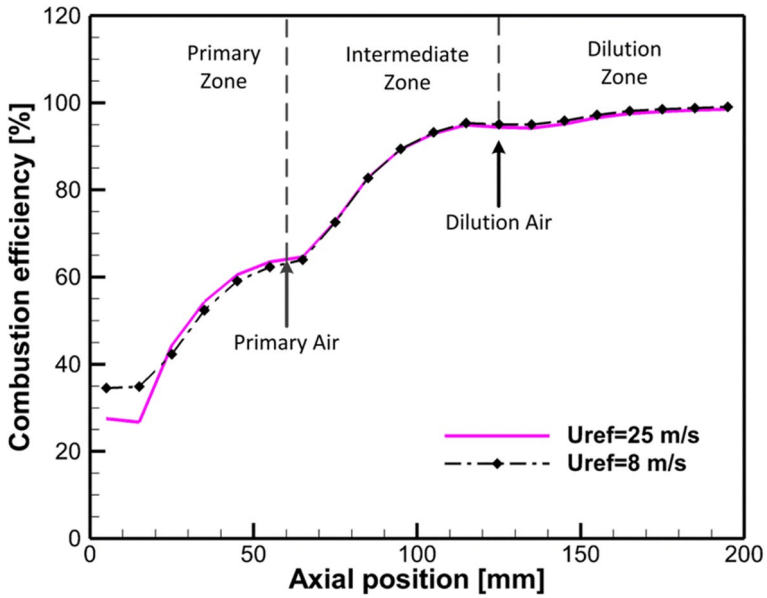

Fig. 10 Profiles of combustion efficiency along the axial direction

on the combustion efficiency occurs on the mixture around the swirler exit. After that, the residence time of the mixture (corresponding to different reference velocities) has a slight effect on the development of the combustion efficiency except for the mixture at the exit of the swirler ($x < 20$ mm). Though the combustion process is "incomplete" in the primary zone, the longer local residence time (corresponding to a lower reference velocity) can not enhance the local combustion. On the contrary, the combustion efficiency even gets a slower rising rate under the case with longer residence time in the primary zone. As the combustion develops downstream, the accumulative combustion efficiency in different cases gets similar in the intermediate zone and the dilution zone. At the outlet, the combustion efficiency is 98.9% and 99.4% for the case with $U_{ref} = 25$ m/s and $U_{ref} = 8$ m/s, respectively.

The effect of reference velocity on the combustion around the swirler exit can be further identified on the reaction progress distribution, shown in Fig. 11. The

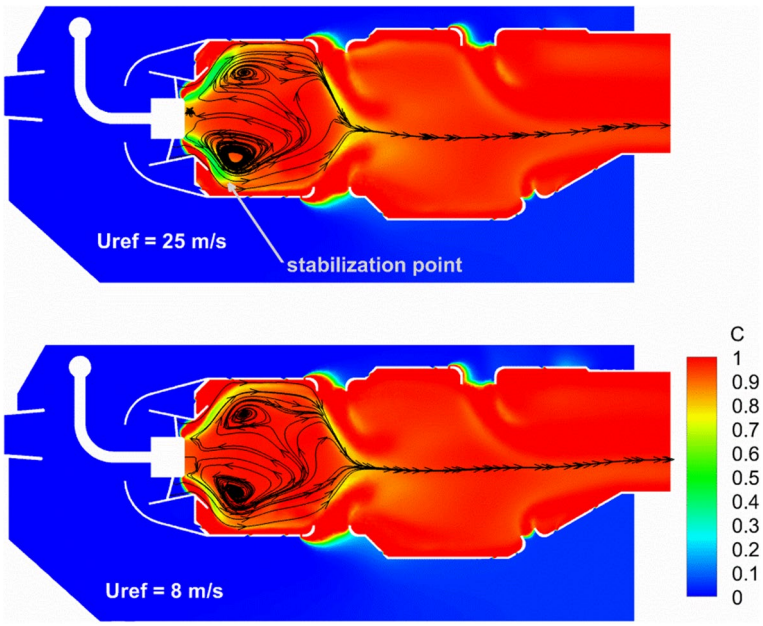

Fig. 11 Distribution of mean reaction progress on the middle plane

nonequilibrium of combustion reaction mainly exists on the base of the swirling flame (the region around the swirler exit) and the upstream shear layer of the primary air jet. The main difference between the two cases is that the nonequilibrium of combustion reaction on the flame base is stronger under the high reference velocity condition; this should be attributed to the shorter residence time for the higher reference velocity. Though the reaction progress is much lower on the flame base in the case with a higher reference velocity, the swirling flame is stabilized at the same position as in the case with a lower reference velocity. The stabilization point is located in the shear layer close to the vortex kernel of the recirculation zone, which indicates that the flame is forcibly ignited by the hot product transported by the recirculation zone. Most of the mixture inside the intermediate zone shows the reaction progress of near 100%, which means that most of the mixture in the intermediate zone is almost at the chemical equilibrium state. Considering the fast increase of the combustion efficiency shown in Fig. 10, the combustion process in this region seems to be controlled by the mixing process rather than the chemical process. In the mixing controlled combustion, the ongoing combustion reactions are resulted from the dissipation of the fuel-rich mixture. This feature seems contrary to the iso-surface of mean stoichiometric mixture fraction distribution in Fig. 8, in which the mixture is in "fuel-mean" state in the intermediate zone. This issue can be understood by the "ensemble average" feature of the RANS method. One can image that the instantaneous combustion field in the intermediate zone is composed by a number of discrete fuel-rich packages, while the ensemble averaged mean mixture fraction is in a fuel-lean state (as shown in Fig. 8) due to the relative low global equivalence ratio in this region.

In summary, the flow and combustion processes show strong self-similarity for the cases with different reference velocities under the present conditions. The simulation results in the present combustor show classic flow and combustion structures for the

swirling combustor. Though the designed reference velocity is relatively high, it slightly affects the flow and combustion structures. This indicates that the local residence time of each zone inside the combustor liner is not the dominant factor in the combustion process. However, the implicated controlling mechanism for the combustion process is interesting, and will be discussed in the next section.

4.2 Discussions on the combustion process

Time scale analysis is carried out to discuss the flame modes in the combustor. Chemical and mixing time scales are involved in the combustion process. The chemical time scale means the required residence time for the combustion reaction if the fuel/air is perfectly mixed; the mixing time scale is the required residence time for fuel/air mixing to be uniform at the molecular level. When the chemical time scale is much smaller than the mixing time scale, the combustion process is controlled by the mixing process. This flame mode is called the diffusion flame. On the contrary, if the mixing time scale is much smaller than the chemical scale, which means the fuel/mixing is perfectly mixed before the combustion reaction, the flame falls into the premixed flame mode. Otherwise, if the chemical time scale and the mixing time scale are comparable to each other, the flame is in the partially premixed mode.

In the FGM combustion model, both the molecular and small scale turbulent mixing of fuel/air mixture are modeled by the dissipation of the mixture fraction variance. Thus, the mixing time scale can be calculated as

$$\tau_{mix} = \frac{\widetilde{z''^2}}{\chi_z}, \tag{7}$$

where $\widetilde{z''^2}$ and χ_z are the variance of the mixture fraction and its dissipation rate, respectively.

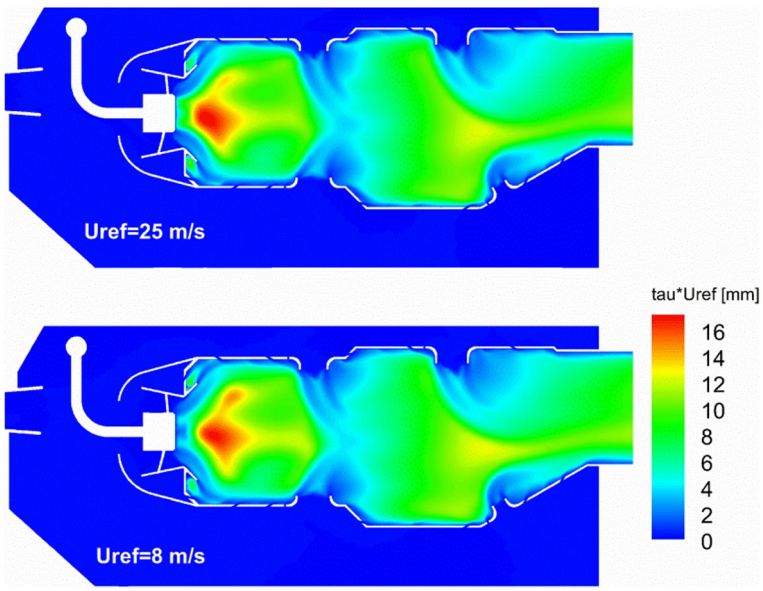

Fig. 12 Product of the mixing time scale and the reference time on the middle plane

The product of the mixing time scale and the reference velocity in different cases are compared in Fig. 12. The defined product appears to have a similar distribution for the cases with different reference velocities, which reveals that the mixing time scale is inversely proportional to the reference velocity. Based on the contours in Fig. 12, the mixing time scales are in the order of 0.5 ms and 1.5 ms for the cases with U_{ref} = 25 m/s and U_{ref} = 8 m/s, respectively.

Based on the definition, the chemical time scale can be evaluated based on the premixed flame under the same thermal conditions. The chemical time scale can be defined as

$$\tau_{chem} = \frac{\delta_l}{s_l}, \tag{8}$$

where δ_l and s_l are the thickness and propagation speed of the laminar premixed flame. Since the chemical time scale only depends on the thermal conditions, the two cases in the present study share the same chemical time scale.

The mean residence time of fuel mixture can be calculated as

$$\tau_{res,f} = \frac{\int_V \overline{\rho}\tilde{z}dv}{\dot{m}_f}. \tag{9}$$

The different time scales are summarized in Table 5. The chemical time scale is much smaller than the mixing time scale. Therefore, the combustion under the present conditions is mainly controlled by the mixing process. In both cases, the fuel mixture residence time is much larger than the mixing time scale. That is the main reason why the reference velocity has a very weak influence on the combustion process. Since the residence time is enough, the mixing process can get a dynamic equilibrium state at each sub-zone of the flow field (e.g., the primary zone, the intermediate zone, and the dilution zone), while the mean flow structure determines the dynamic equilibrium state for mixing.

To further verify the above conclusion, the production and dissipation of mixture fraction variance at different axial positions are integrated and plotted in Fig. 13. Overall, the production rate and the dissipation rate are comparable to each other; the net production is much smaller than the production rate and the dissipation rate in magnitude. Dynamic balance is achieved at each interface of the functional zones (e.g., $x \approx 60$ mm and $x \approx 120$ mm), which indicates that quasi-equilibriums for mixing are achieved at the outlet of the primary and intermediate zones. Downstream of the equilibrium point, the balance between production rate and dissipation is broken by the newly added air jet (e.g., the primary air jet and the dilution air jet).

Table 5 Different time scales in the combustion process

	$\tau_{res,f}$	τ_{chem}	τ_{mix}
Case 1	5.5 ms	~0.09 ms	~0.5 ms
Case 2	17.9 ms	~0.09 ms	~1.5 ms

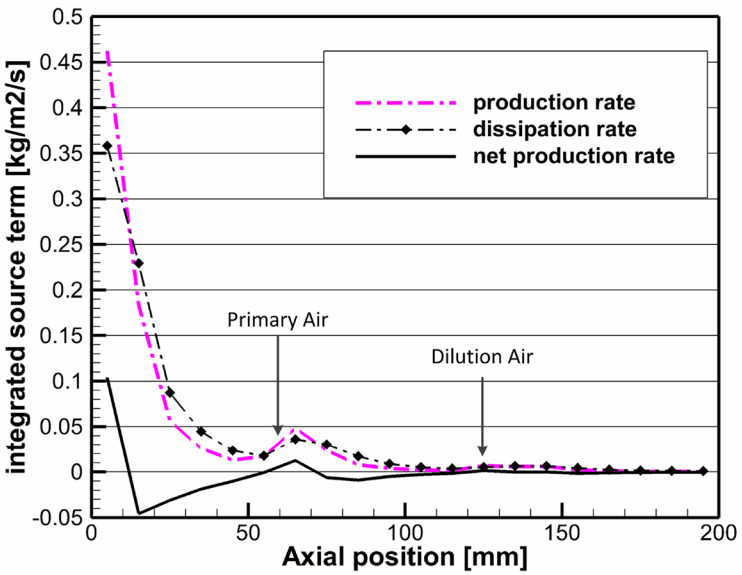

x	net prod
5	1.04E-01
15	-4.57E-02
25	-3.11E-02
35	-1.89E-02
45	-1.03E-02
55	-7.21E-04
65	1.23E-02
75	-6.42E-03
85	-8.98E-03
95	-5.04E-03
105	-2.98E-03
115	-1.81E-03
125	1.35E-03
135	-1.47E-04
145	-2.04E-04
155	-1.75E-03
165	-1.26E-03
175	-8.38E-04
185	-6.01E-04
195	-5.04E-04

Fig. 13 Integrated production rate and dissipation rate of mixture fraction variance along the axial direction

The mixing efficiency is involved to further understand the mixing process. For a given axial section, the mixing efficiency can be expressed as [28]

$$\eta_{mix} = \frac{\int_A \int_{z=0}^{1} \overline{\rho}\widetilde{\vec{U}}\alpha(z)p\left(z;\widetilde{z},\widetilde{z''^2}\right)dz \cdot d\vec{A}}{\int_A \overline{\rho}\widetilde{\vec{U}}\widetilde{z} \cdot d\vec{A}}, \tag{10}$$

with

$$\alpha(z) = \begin{cases} z,\ z \le z_{st} \\ (1-z)\dfrac{z_{st}}{1-z_{st}},\ z > z_{st} \end{cases}, \tag{11}$$

where, $p\left(z;\tilde{z},\widetilde{z''^2}\right)$ is the PDF of the mixture fraction used in the combustion model.

The mixing efficiency at different axial positions is compared with the combustion efficiency and the fuel-mass-weighted mean reaction progress in Fig. 14. The mean reaction progress is weighted by the fuel-mixture, which is expressed as

$$C_{mean} = \frac{\int_A \overline{\rho}\widetilde{\vec{U}}\tilde{z}\tilde{c} \cdot d\vec{A}}{\int_A \overline{\rho}\widetilde{\vec{U}}\tilde{z} \cdot d\vec{A}}. \tag{12}$$

As shown in Fig. 14, the combustion efficiency even exceeds the mixing efficiency around $x = 45$ mm. Based on the physical definitions, the combustion efficiency should be smaller than the mixing efficiency with $c < 1$, and equal to the mixing efficiency when $c = 1$. However, this relationship of $\eta_c = \eta_{mix}$ at $c = 1$ could be influenced by several factors. Firstly, the mixing efficiency is targeted on the mass mixing, while the combustion

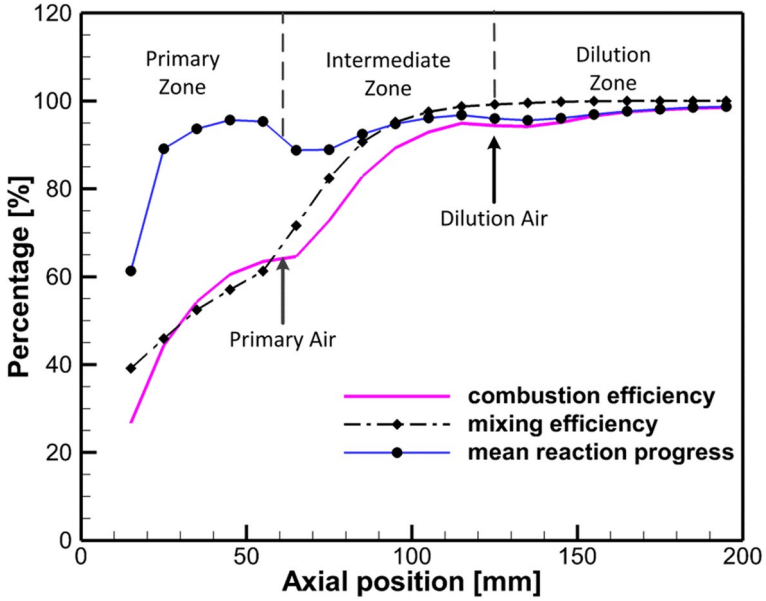

Fig. 14 Profiles of mixing efficiency along the axial direction

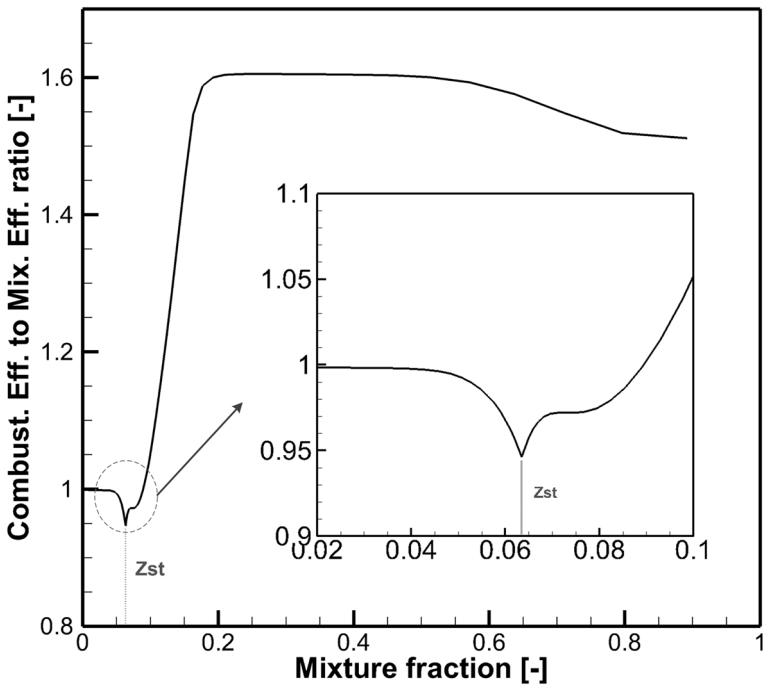

Fig. 15 The ratio of combustion efficiency to the mixing efficiency versus mixture fraction at $c = 1$ sampled from the FGM table

efficiency is targeted on the thermal heat release. The non-linear heat-release during the fuel oxidizing process may break the equality on the fuel-rich state (mixing and fuel oxidization are incomplete). Secondly, the reversible feature of the combustion reaction can lead $\eta_c < \eta_{mix}$ even at $c = 1$. These effects are shown in Fig. 15. The present definitions

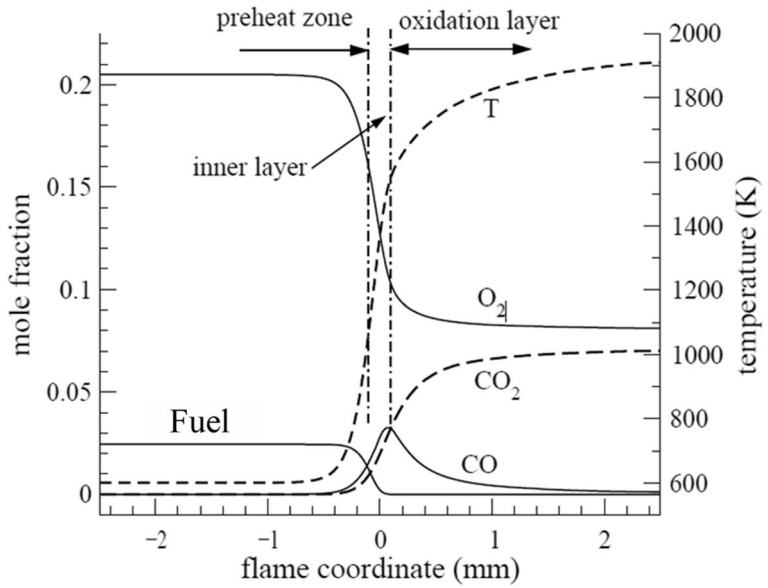

Fig. 16 Structure of 1-D premixed flame

make the combustion exceed the mixing efficiency in the fuel-rich mixture; the highest combustion efficiency of the stoichiometric mixture is only 94% due to the effect of the reversible reaction. As shown in Fig. 14, the mixing efficiency exhibits a similar trend to the combustion efficiency in the primary zone and the intermediate zone, which implies the mixing-controlled nature of the combustion process in these regions. However, some roles of the chemical nonequilibrium in the combustion process can still be identified by comparing the combustion efficiency with the sectional mean reaction process. For example, the low reaction process at the swirling flame base ($x \approx 15$ mm) and the primary holes ($x \approx 70$ mm) makes the combustion efficiency lower than the mixing efficiency. In the dilution zone, the mixing of the fuel-rich mixture has been completed ($\eta_{mix} \approx 100\%$), and the combustion efficiency inhibits the similar trend to the mean reaction progress, which implies the controlling factor of the combustion shifts from mixing to the chemical reaction in this region.

As mentioned above, all of the mixture in the dilution zone is in a fuel-lean state. Therefore, the chemical reaction in this region happens in the stratified lean premixed mixture. However, the combustion reaction in this region is different to the conventional premixed flame. The premixed flame is a fast chemical process coupled with species and heat diffusion happening in a thin sheet [19]. As shown in Fig. 16, the whole flame layer can be divided into the preheat zone, inner layer (also known as "reaction zone"), and oxidation zone (also known as "post flame zone"). The heat and radicals can feed back from the reaction zone to the preheat zone, which drives the flame front propagating towards the unburnt side. There are several differences between the combustion process in the dilution zone and the conventional premixed flame. Firstly, the reaction progress in this reaction varies in the range of $c = 0.95 - 1.0$, which only corresponds to the post flame zone of the conventional premixed flame (as shown in Fig. 16). Secondly, the reaction rate is much slower than the conventional premixed flame due to

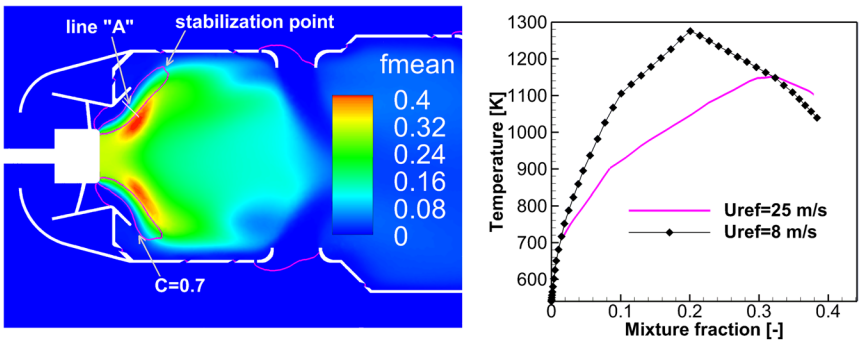

Fig. 17 The mixing and reaction on the flame base. **a** Distribution of mixture fraction around the swirler exit. **b** Temperature versue mixture fraction sampled on line "A"

the missing of supporting from the highly active reaction in the reaction zone. Thirdly, due to the slow reaction rate, the reaction will continue in a considerable volume rather than a thin sheet. In summary, the chemical reaction process in the dilution zone under the present conditions prefers to the spatially homogeneous reactions in the perfectly-stirred reactor (PSR) rather than to a premixed flame behavior. Therefore, the reaction process is strongly dependent on the residence time of the mixture. This is why the combustion efficiency at the outlet for the case with a lower reference velocity is slightly higher than that in the case with a higher reference velocity.

Finally, the mixing and reaction properties around the swirler exit are plotted in Fig. 17 to understand the combustion process on the flame base. Based on Fig. 17a, Fig. 7, and Fig. 11, the flame base (the non-equilibrium region around the swirler exit) is on the mixing layer between the fuel-rich mixture ($z \sim 0.35$) and the fresh air. The fuel evaporates in the fuel-rich region in the chemical equilibrium state ($c \sim 1$), and results in the high mixture fraction region ($z > 0.3$) around the flame base. The mixture across the mixing layer is sampled (marked as "line A" in the figure), and plotted in Fig. 17b. The temperature shows a non-monotonous profile with the mixture fraction across the sampled line. This feature indicates that slow oxidization reactions are occurring in the mixing layer upstream of the flame stabilization position. These reactions inside the mixing layer are like the auto-ignition process of a non-premixed flamelet [29], in which the fuel side composition is set up as a fuel-rich mixture ($z \sim 0.35$). The auto-ignition reaction is relatively slow and is dependent on the residence time; thus the reaction progress at the given position decreases with the reference velocity. Although the auto-ignition reaction is ongoing in the mixing layer, the residence time is not enough for the completion of auto-ignition for both cases under the present conditions, and the reactive mixing is finally ignited by the hot product with a lower mixture fraction transported from the vortex kernel.

Based on the above discussions, the experience of the fuel vapor inside the combustor could be summarized in Fig. 18. The fuel is injected into the hot rich product mixture, and evaporates due to the heating by the product (state "S1"). After that, two branches in the (z, η_c) space could be experienced by the fuel mixture. In the first branch, the fuel mixture is first slowly oxidized by the auto-ignition of the non-premixed flame in the mixing layer between the rich product and the fresh air (path "P1"), and then is forcibly

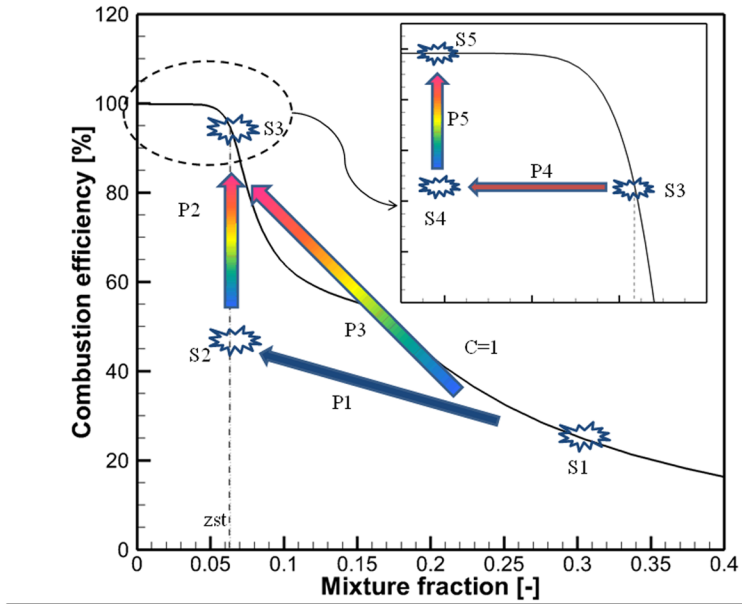

S1: original evaporated fuel in fuel-rich region	P1: auto-ignition of non-premixed flame
S2: non-equilibrium mixture at flame base	P2: partially premixed combustion at flame base
S3: equilibrium mixture in stoichiometric state	P3: combustion of diffusion flame
S4: non-equilibrium mixture in fuel-lean state	P4: dilution of the stoichiometric production
S5: equilibrium mixture in fuel-lean state	P5: slow oxidization in fuel-lean mixture

Fig. 18 Sketch for the oxidization process of fuel vapor inside the combustor

ignited and combusted at the partially premixed flame base (path "P2"). In the second branch, the fuel is combusted in the diffusion flame mode, in which the oxidization reaction is synchronous with the fuel/air mixing process (path "P3"). The above two branches share the same end state, which is the chemical equilibrium mixture in the stoichiometric state (state "S3"). Since the combustion reactions are reversible, the fuel in state "S3" can not be oxidized completely due to the existence of intermediate species. The mixture is diluted into a fuel-lean state (state "S4") by the fresh air through the dilution holes. The fuel is further oxidized when the equilibrium point of the reactions is shifted towards the product side in the dilution zone (path "P5"). Around 4% of the chemical heat is released during path "P5". Considering the required combustion efficiency (> 99%) from the aero-engine design [11], the slow oxidization in the dilution zone is non-negligible during the design of the combustor.

5 Conclusions

The mixing and combustion processes in a small-scale gas turbine combustor were numerically investigated using the Flamelet Generated Manifold (FGM) model based on the Reynolds Averaged Navier–Stokes (RANS) method. The numerical methods were evaluated based on a model combustor and the sensitivity study on the θ-parameter. Two cases with different reference velocities were considered in the study. The combustion modes inside the combustor were analyzed. A sketch map on phase space of mixture fraction and combustion efficiency was proposed to explain

the mixing and reaction processes of the injected fuel. The main conclusions are summarized as follows:

- The flow and combustion fields show self-similarity for the cases with different reference velocities under the present conditions. The main difference is on the nonequilibrium in the mixing layer upstream of the flame stabilization point.
- In general, the combustion process exhibits the mixing-controlled feature. However, partially premixed combustion appears in part of the flame, particularly at the base of the swirling flame.
- The residence time of the fuel mass inside the combustor is much longer than the required time for micro-mixing and chemical reaction of fuel/air mixing. Thus, the macroscopic combustion properties (e.g., the sectional combustion efficiency) at the end of each sub-zone (e.g., the primary zone, intermediate zone, and dilution zone) are dominated by the mean flow structures.
- Due to the reversible feature of the combustion reactions, the fuel can not be fully oxidized in the primary and intermediate zones, though air is enough. Part of the fuel is further oxidized in the dilution zone, contributing to adding new fresh air from the dilution zone. This oxidization is a slow chemical controlled process, which is strongly dependent on the residence time. Though this portion of fuel oxidization is very little (~4%), it is non-negligible in the combustion organization during the combustor design.

Acknowledgements
Not applicable.

Authors' contributions
The research output comes from joint efforts. All authors read and approved the final manuscript.

Funding
This work was supported by the National Natural Science Foundation of China (Grant Nos. 51706238, 91941301).

Availability of data and materials
The data that support the findings of this study are available from the corresponding author upon reasonable request.

Declarations

Competing interests
The authors declare that they have no competing interests.

Received: 5 January 2023 Accepted: 20 June 2023
Published online: 05 September 2023

References

1. Candel S, Durox D, Schuller T et al (2014) Dynamics of swirling flames. Annu Rev Fluid Mech 46:147–173
2. Kao YH, Denton M, Wang XH et al (2015) Experimental spray structure and combustion of a linearly-arranged 5-swirler array. In: Proceeding of the ASME turbo expo 2015: turbine technical conference and exposition. Montreal, 15-19 June 2015. Volume 4A: combustion, fuels and emissions. ASME, New York, V04AT04A038
3. Willert C, Jarius M (2002) Planar flow field measurements in atmospheric and pressurized combustion chambers. Exp Fluids 33:931–939
4. Xiao YL, Wang ZP, Lai ZX et al (2018) Flow field and species concentration measurements in the primary zone of an aero-engine combustion chamber. Adv Mech Eng 10:1–11
5. Zarzalis N, Ripplinger T, Hohmann S et al (2002) Low-NOx Combustor Development pursued within the scope of the Engine 3E German national research program in a cooperative effort among engine Manufacturer MTU, University of Karlsruhe and DLR German Aerospace Research Center. Aerosp Sci Technol 6(7):531–544
6. Meier U, Heinze J, Freitag S et al (2012) Spray and flame structure of a generic injector at aeroengine conditions. J Eng Gas Turb Power 134(3):031503

7. Jones WP, Marquis AJ, Vogiatzaki K (2014) Large-eddy simulation of spray combustion in a gas turbine combustor. Combust Flame 161:222–239
8. Gao DS, Jin J, Shen S et al (2021) Evolution analysis of high temperature zones in a double-swirled model combustor. J Combust Sci Technol 27(4):434–442 (in Chinese)
9. Benim AC, Iqbal S, Meier W et al (2017) Numerical investigation of turbulent swirling flames with validation in a gas turbine model combustor. Appl Therm Eng 110:202–212
10. Lilley DG (2008) Swirl and lateral injection for improved mixing and combustion. In: Proceedings of the ASME 2006 power conference. Atlanta, 2-4 May 2006. ASME, New York, p 523–530
11. Lefebvre AH, Ballal DR (2010) Gas turbine combustion: alternative fuels and emissions, 3rd edn. CRC Press, Boca Raton
12. Zhao Y, He X, Li M et al (2021) Ignition, efficiency and emissions of RP-3 kerosene in a three-staged multi-injection combustor. Fuel Process Technol 213:106635
13. Ding G, He X, Zhao Z et al (2015) Effect of different triple swirlers on the performance of a triple swirler combustor. Proc Inst Mech Eng G J Aerosp Eng 229(1):26–37
14. Kong F, Li T, Cheng C et al (2022) Modeling of spray flame in gas turbine combustors with LES and FGM. Fuel 325:124756
15. Van Oijen JA, De Goey LPH (2000) Modelling of premixed laminar flames using Flamelet-Generated Manifolds. Combust Sci Technol 161(1):113–137
16. Zhou Y, Le J, Huang Y (2018) LES of combustion flow field in a practical aeroengine combustor with two-stage counter-rotating swirler. J Propuls Technol 39(7):1576–1589
17. Patwardhan S, Nakod P, Orsino S et al (2021) Prediction of CO emission index for aviation gas turbine combustor using flamelet generated manifold combustion model. In: Proceedings of the ASME turbo expo 2021: turbomachinery technical conference and exposition. Virtual, 7-11 June 2021. Volume 3B: combustion, fuels, and emissions. ASME, New York, V03BT04A008
18. ANSYS Inc (2022) Ansys: engineering simulation software. https://www.ansys.com. Accessed 20 Jan 2023
19. Peters N (2000) Turbulent combustion. Cambridge University Press, Cambridge
20. Ihme M, Shunn L, Zhang J (2012) Regularization of reaction progress variable for application to flamelet-based combustion models. J Comput Phys 231(23):7715–7721
21. Yadav R, Nakod P (2015) Numerical computation of a turbulent lifted flame using flamelet generated manifold with different progress variable definitions. In: Proceedings of the ASME 2015 gas turbine India conference. Hyderabad, 2-3 December 2015. ASME, New York, V001T03A008
22. ANSYS Inc (2022) ANSYS Fluent theory guide. https://ansyshelp.ansys.com/account/secured?returnurl=/Views/Secured/corp/v192/flu_th/flu_th.html. Accessed 20 Jan 2023
23. Dagaut P (2002) On the kinetics of hydrocarbons oxidation from natural gas to kerosene and diesel fuel. Phys Chem Chem Phys 11(4):2079–2094
24. Freitag S, Meier U, Heinze J et al (2010) Measurement of initial conditions of a kerosene spray from a generic aero-engine injector at elevated pressure. In: Proceedings of the 23rd annual conference on liquid atomization and spray systems, Brno, 6-8 September 2010
25. Meier UE, Wolff-Gaßmann D, Stricker W (2000) LIF imaging and 2D temperature mapping in a model combustor at elevated pressure. Aerosp Sci Technol 4(6):403–414
26. Aviation Industry Department of China (1987) Aero-engine gaseous pollutant sampling and measurement procedures. Aviation Industry Standard HB 6117–87
27. Jiang P, He X (2020) Performance of a novel mixed-flow trapped vortex combustor for turboshaft engine. Aerosp Sci Technol 105:106034
28. Watanabe J, Kouchi T, Takita K et al (2011) Large-eddy simulations of hydrogen and ethylene injections into a supersonic crossflow. 47th AIAA/ASME/SAE/ASEE joint propulsion conference & exhibit, San Diego, 31 July - 3 August 2011
29. Mastorakos E (2009) Ignition of turbulent non-premixed flames. Prog Energy Combust Sci 35(1):57–97

Publisher's Note